Energy Conversion and Management: X 15 (2022) 100253

Contents lists available at ScienceDirect

Energy Conversion and Management: X

journal homepage: www.sciencedirect.com/journal/energy-conversion-and-management-x

A PV powered DC shunt motor: Study of dynamic analysis using maximum power Point-Based fuzzy logic controller

Nagy Osman [a], Haris M. Khalid [a], Tha'er O. Sweidan [a], Mohammed I. Abuashour [b], S.M. Muyeen [c,*]

[a] Department of Electrical and Electronics Engineering, Higher Colleges of Technology, Sharjah 7947, United Arab Emirates
[b] Electrical Engineering Department, Renewable Energy Center, Hashemite University, Zarqa 13115, Jordan
[c] Department of Electrical Engineering, Qatar University, Doha 2713, Qatar

ARTICLE INFO

Keywords:
DC shunt motor
DC-to-DC boost converter
Fuzzy logic controller
Fuzzy membership function
Fuzzy rules
Maximum power point tracking
Performance analysis
Photovoltaic panel
Photovoltaic system
Solar arrays
Transient analysis

ABSTRACT

Solar cells absorb sun light and convert it into electricity. However, the infrastructure of solar cells, their initial cost, energy conversion and efficiency could raise some challenges and concerns. This is because of the current–voltage properties of solar cells which are strongly dependent on the solar radiation and the ambient temperature level. This further causes fluctuations in the photovoltaic (PV) output power. In this article, a novel scheme is proposed to improve the PV system efficiency. This is achieved by using tracker techniques to calculate the maximum power point tracking (MPPT) where the energy can be safely passed to the load under suitable conditions. The scheme is further enhanced by investigating a PV generator and a direct-current (DC) shunt motor using a fuzzy logic controller (FLC) method for monitoring and tracking the maximum power point. A power electronics system based on boost DC-to-DC converter is used along with the PV module to raise the performance by the shift of the converter control input duty cycle. Evaluations were made to analyze the dynamical behavior and the steady state performance of the direct current shunt motor obtained from the PV module using MATLAB SIMULINK.

Introduction

The high needs of electrical energy and thus environmental issues have been escalated due to the unusual growth of global population. The manufacturing side has increased the attention to the advantages of using clean energy power sources such as solar PV, wind turbine, and biomass, which are named as the pollution-free options [1].

Solar Irradiation, MPPT, and scope of this work

Solar electrical energy is obtained by the steady conversion of external sunlight into electrical energy. However, to carry out this conversion process, the solar cells must provide a stable voltage. Several efforts have been made to provide stable voltage in the presence of environment effects [2,3]. Because of the solar irradiation intermittency, the cells cannot meet the full and stable voltage supplied to the load and the maximum output will still be less than the system's true power. To solve this problem, several MPPT techniques have been invented. MPPT controller enables the larger electrical energy input and output from the PV system by tracking and monitoring various parameters at the PV module to make it run at its full performance [4]. To address the photovoltaic system's higher electrical energy needs, researchers developed several MPPT techniques such as factional short circuit current, proportional integral (PI) controller and the method of considering the open circuit voltage to control the converter system which is called fractional open-circuit voltage [5]. Utilization of MPPT as a controller to improve the performance of the PV panel connected to different types of loads is presented in these works. However, to utilize MPPT controller to achieve the steady state stability is not studied, which is the main scope of this work.

MPPT methods, DC shunt motor, and motivation of this paper

The perturbation and observation (P and O) technique is investigated as an MPPT method and evaluated by taking into account big signal stability tests for distributed power systems by three phases symmetrical

* Corresponding author.
E-mail address: sm.muyeen@qu.edu.qa (S.M. Muyeen).

https://doi.org/10.1016/j.ecmx.2022.100253
Received 3 March 2022; Received in revised form 15 June 2022; Accepted 16 June 2022
Available online 17 June 2022

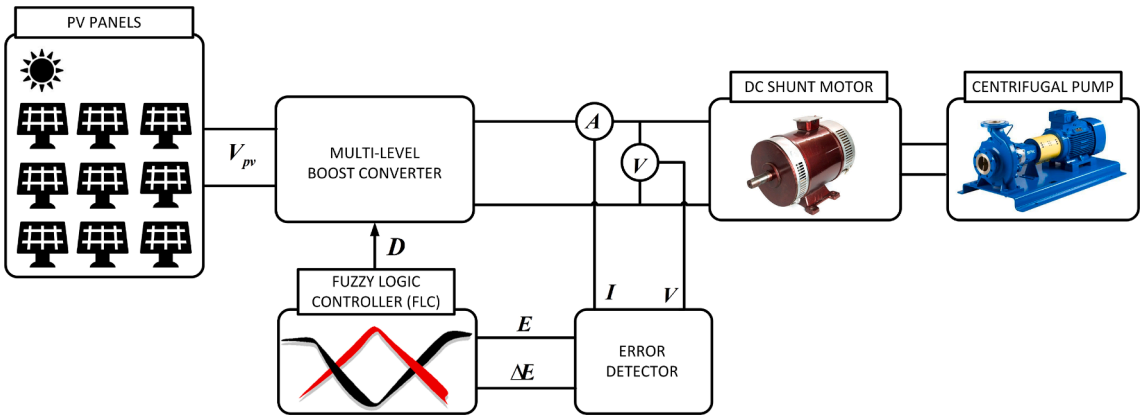

Fig. 1. Schematic diagram of the proposed scheme.

fault on the mid length of transmission power phases. The PV module here is affected by different solar radiation levels and the system simulation results reflect the facts of highly PV penetrated grid sustainability [6]. The system model is introduced and measured for various radiations to demonstrate the dynamical/transient and steady state conditions for fixed magnet, parallel, and series motors operated by PV module. The findings are comparable to those obtained by powering the motors with a fixed voltage source, revealing strong consistent and a great variety of harmony operating points [7]. The dynamical and steady state analysis of direct current machines powered by a PV module at various radiation stages and motor toque of load is investigated in [8]. As a preliminary study, the transient behavior of the different MPPT techniques of different applications including a combined alternating current (AC) motors and DC motors is inspected at various radiation levels. Moreover, the compensating mechanism of the system has been achieved by calculating the optimal load torque for the different isolation levels. The goal of the work was to examine the system's behavior at different solar radiation levels [5]. In Sweidan et al. [9], the authors describe a PV generator that drives a direct current shunt motor and uses a fractional open circuit voltage technique to monitor power to achieve and generate extreme power from a PV generation system. The dynamical/transient and steady state behavior of a direct current shunt motor powered by a PV module generator have been identified at various isolation rates. Several MPPT methods have been implemented to improve the DC shunt motor performance while employing PV panel. However, their responses did not show the ability to get an efficient dynamic performance under the effect of load torque variations, which is the main motivation of this paper. This work focuses on achieving both stead state and dynamic stability of DC shunt motor.

Main contribution of this paper

The main contribution of this paper is to design a robust MPPT controller based on a fuzzy inference system and using a power electronics system with a DC-to-DC boost converter to achieve and improve the DC shunt motor's dynamic performance and stability. The DC shunt motor dynamic performance is analyzed while employed by the PV panel and considering different load torque variations. The schematic diagram of the proposed scheme can be seen in Fig. 1.

Formation of this paper

The formation of the remaining paper is organized as follows; In Section 2, proposed formulation with system configuration is presented. This involves subsections on control panels, FLC, DC-to-DC boost converter, and DC shunt motor. Section 3 shows implementation and evaluation. Finally, conclusion is presented in Section 4.

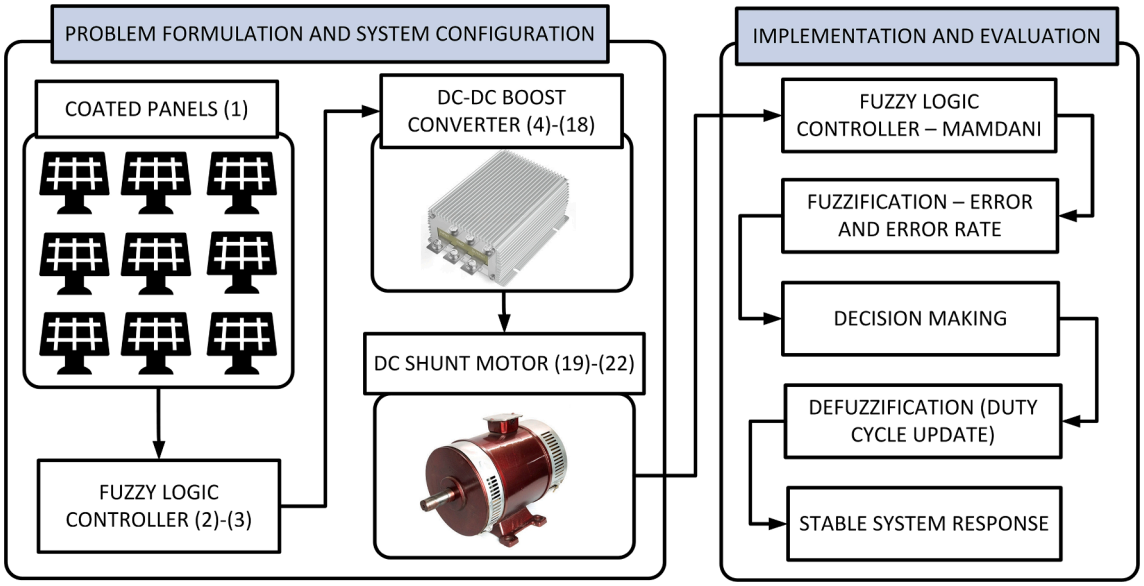

Fig. 2. Problem formulation and its implementation layout diagram.

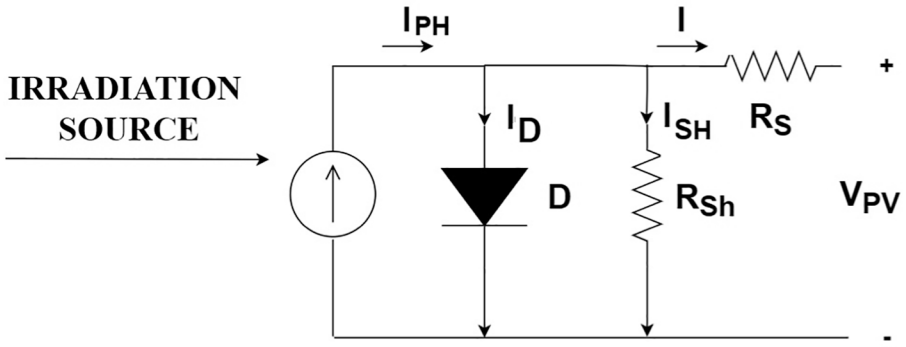

Fig. 3. PV cell equivalent circuit.

Problem formulation and system configuration

The problem formulation and system configuration are expressed in this section. An overview of the proposed scheme can be seen in Fig. 2. It begins with mathematical representation of current/voltage characteristic of PV cell in (1). The fuzzy logic controller is described and defined in (2)–(3). The DC-DC boost converter is expressed and derived in (4)–(18). The DC shunt motor and its equivalent circuit is expressed in (19)–(22).

Coated panels

PV cells, semiconductor, and sunlight

The sunlight may be mirrored, refracted, or possibly transmitted through the cell when it passes on a PV cell. The PV cell is made of semiconductor material which conducts electricity. Though a semiconductor is better than dielectric, it is not a great conductor like metal. PV cells are made up of a variety of these semiconductor materials. When exposed to sunlight, a semiconductor absorbs the energy and converts it into electrons. This additional energy allows electrons to pass as an electrical charge (current) through the material. This current is obtained through highly conductive metal contacts (the grid-like lines on solar cells). It is further utilized to supply energy to consumer homes and the electric grid utility. The efficacy of a PV panel is proportionate to the amount of energy produced by the cell. This is equivalent in comparison to the energy emitted by the reflective light, indicating how efficient the cell is at transferring energy from one type to another. The amount of power produced by PV cells is determined by the type of available light as well as the multiple performance attributes of the cell. The bandgap of solar panel semiconductors is a significant property that determines what wavelengths the substance can absorb and transfer to electric power. If the bandgap of the semiconductor suits the wavelengths appearing on the PV panel, the cell can effectively use all the available energy [10].

Equivalent circuit diagram and its mathematical representation

The equivalent circuit diagram of semiconductor PV cell is shown in the Fig. 3 below [10].

The general mathematical representation that describes the current/voltage characteristic of the PV cell is given below:

$$I = I_{PH} - I_D[q(V_{PV} + IR_S)/nKT - 1] - [V_{PV} + IR_S/R_{SH}] \quad (1)$$

where I represent the output current, I_{PH} is the generated current source, q is the electron charge, V_{PV} is the photovoltaic open circuit voltage, R_S is the series resistance of equivalent PV cell open circuit current, n is the number of series connected cells. K is the Boltzman constant, T is the ambient temperature, and R_{SH} is the short circuit resistance.

Fuzzy logic controller (FLC)

Fuzzy sets

The theory of fuzzy sets as an inspiration for the use of human practice knowledge [11]. Fuzzy system incorporates pro user expertise into the controller design and attempts to gather further data that is gathered through observing experienced users' habits. Fig. 4 describes four key components of an FLC:

1) The Value-to-Mapper (Fuzzification): This map crisp values to a subset.
2) The Ruleset: The ruleset implements the actions through logical conditions and statements (IF-THEN).
3) The Inference System: This system converts input into output, and
4) The Defuzzification (Convert Fuzzy Sets System): This system blends values to sets of fuzzy statements.

There are statements about the FLC which that can be interpreted as fuzzy sets. The fuzzy output duty cycle controller is obtained by inference behavior either by making an inference about something or deducing something from what was previously obtained [10,12].

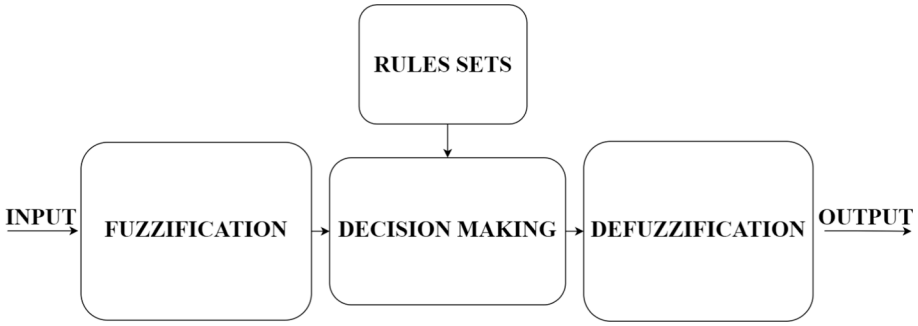

Fig. 4. Fuzzy system.

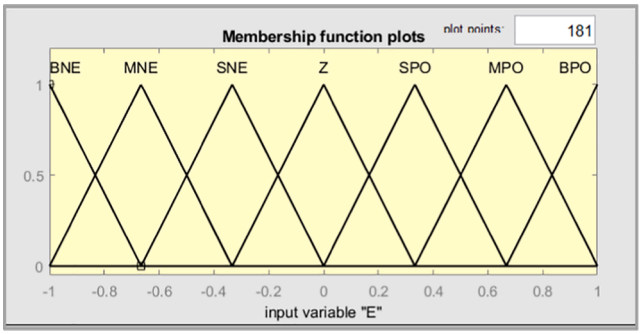

Fig. 5. Membership function of input Error E.

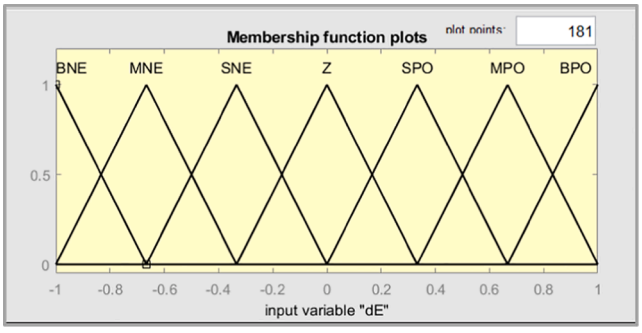

Fig. 6. Membership function of input error rate ΔE.

Fuzzy membership Function:

The fuzzy system membership functions identified with the FLC variables are mostly linear functions. The proposed implementation here is built on triangular and trapezoid functions. Note the triangular linear functions are of relevance in this study in the development of fuzzy controllers. In addition to all fuzzy logic processes, the fuzzy sets membership functions are mainly based on trials and errors method. Trial and error processes should be in a repetitive manner until getting satisfactory results with respect to the input data sets.

Duty cycle and membership function configuration

With the increase of power, the duty cycle should change. However, if the power starts to fall from the targeted value, the duty cycle should be reversed in the other direction [12–15]. The MPPT is designed to ensure that the controlling task continuously displace the operating point of the solar panel array as close as possible to maximum power point. Fuzzy set of Mamdani is used as an inferencing system here. This employs a set of predefined fuzzy rules [16]. The error value (E_t) and the error rate (ΔE_t) are the fuzzy controller inputs. These are stated as:

$$E_t = (P_t - P_{t-1})/(V_t - V_{t-1}) \tag{2}$$

$$\Delta E_t = E_t - E_{t-1} \tag{3}$$

where error E_t is the difference between the desired power/voltage values and the measured one. The change in error ΔE_t is the rate of change of the error value. This indicates the accuracy of the controller while moving towards the desired point. The time of each sample is denoted by t. The instant power of PV generator is denoted by P_t. The instantly equivalent voltage is denoted by V_t. These values are selected to ensure the offset of the instantaneous value of E_t from the maximum power actual location. Note the pulse width modulation (PWM) output signal is the controlled waveform here and it is sent to the boost DC-to-DC converter to control the DC shunt motor input power. The Mamdani-based defuzzification method is then used with centre of area to find the exact suitable of (D) as a crisp performance [14,15].

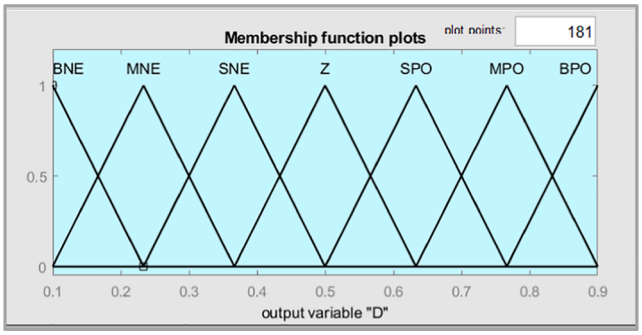

Fig. 7. Membership function of output duty cycle D.

Table 1
Fuzzy rules.

ΔE / E	BNE	MNE	SNE	ZE	SPO	MPO	BPO
BNE	Z	SNE	MNE	BNE	BNE	BNE	BNE
MNE	SPO	Z	SNE	MNE	BNE	BNE	BNE
SNE	MPO	SPO	Z	SNE	MNE	BNE	BNE
Z	BPO	MPO	SPO	Z	SNE	MNE	BNE
SPO	BPO	BPO	MPO	SPO	Z	SNE	MNE
MPO	BPO	BPO	BPO	MPO	SPO	Z	SNE
BPO	BPO	BPO	BPO	BPO	MPO	SPO	Z

Figs. 5–7 show the configuration of the membership functions of the inputs (error and error rate) and output (duty cycle) variables. The range of error values is from –1 to +1 W/V. The linguistic variables are: 1) big negative (BNE), 2) medium negative (MNE), 3) small negative (SNE), 4) zero (Z), 5) small positive (SPO), 6) medium positive (MPO), and 7) big positive (BPO). The range of error rate is from – 1 to +1 W/V. And its linguistic variables are: 1) BNE, 2) MNE, 3) SNE, 4) Z, 5) SPO, 6) MPO, and 7) BPO. The pulse width modulator (PWM) signal driver (duty cycle) has a range of 0.1–0.9 and has linguistic variables of BNE, MNE, SNE, Z, SPO, MPO, and BPO. Table 1 shows a list of fuzzy logic controller rules with fuzzy system of error value (E) and error rate (ΔE) as inputs. The duty cycle is the outcome of the rule set, D.

DC-to-DC boost converter

Switch mode and DC voltage supply

In switch-mode, the converters are commonly placed in the DC-to-DC regulators. The DC voltage supplied to these converters may be from a PV series which causes fluctuations in the output. If the desired DC voltage and the average input voltage do not match, the converters must be adjusted. The output signal of DC-to-DC converter is continuously adjusted based on the amount of power received from the source. It is further adapted to pass it perfectly to the load input. From an energy standpoint in a PV system, output electrical signal management in a DC-to-DC converter is accomplished by continuously changing the required energy consumed from the power source and passed to the load. It is further regulated by the relative durations of absorption and injection intervals.

Switching cycle

A switching cycle is made of two essential steps, which are: 1) energy consumption, and 2) insertion. Intuitively, if the energy storage capability of converter is insufficient or the swapping time is extremely long, the chopper may have transferred all the generated electrical energy to its electrical load until the next loop starts. This results in a cycle update for the next duration in which the chopper circuit remains static [17–19].

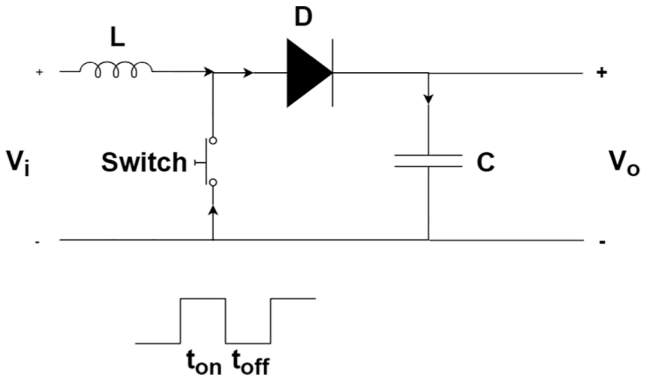

Fig. 8. Equivalent circuit of boost converter.

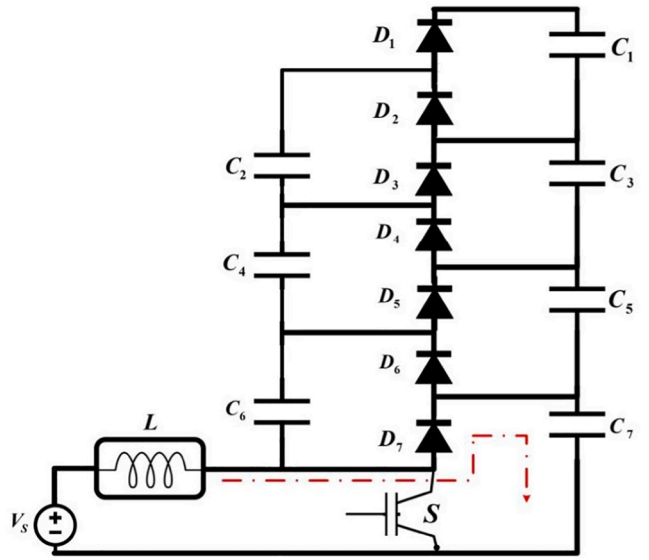

Fig. 9. Four level boost converter.

Operating models of boost converter

This section describes the operating modes of boost converter.

Fig. 8 depicts a graphical model of the boost converter. Four external components are required for the DC-to-DC boost converter, which are: 1) an inductor, 2) an electronic switch, 3) a semiconductor diode, and 4) an output capacitor.

There are mainly two operating conditions and modes in continuous conduction mode of DC-to-DC converters.

1) *First Mode:* The first mode is called as the mode 1. It starts when the insulated gate bipolar transistor (IGBT) switch is turned on at the initial time, $t = 0$. The operation continues during the on-time denoted as t_{on}. The current in the inductor is higher than zero which increases linearly.
2) *Second Mode:* The second operating mode is called as the mode 2. It starts when the switch is turned off at the end of the on-cycle. The operation remains off during the off time denoted as t_{off}. Here the inductor voltage is equal to the input voltage. During the next step, the inductor current decreases until the switch is turned-on again. The voltage across the inductor equals the difference between the input and output voltages during the on-time. Because the time integral of the inductor voltage over one time span must be zero in steady state, the output voltage can be calculated as shown in (4) and (5).

$$V_i t_{on} + (V_i - V_0) t_{off} = 0 \tag{4}$$

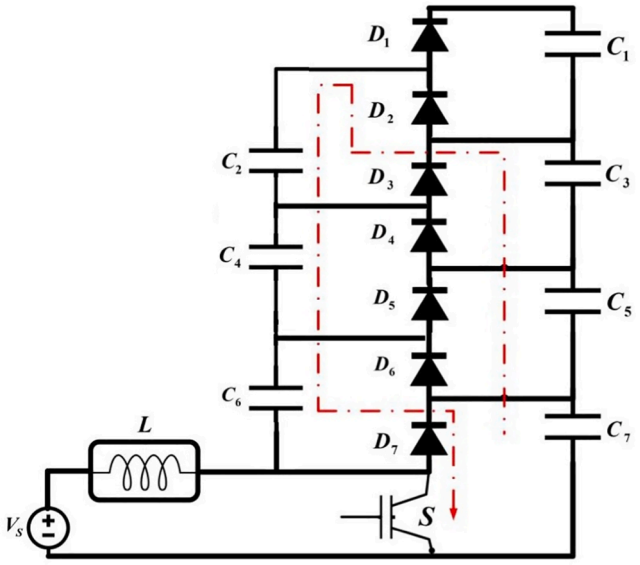

Fig. 10. Four level boost converter - During the ON mode (switch ON) the odd numbered capacitors charge the even ones.

where V_i is the electrical input voltage of the chopper circuit, and V_o is the chopper output voltage. t_{on} is the time when the switch is in the operating mode and in turned-on condition. t_{off} is the time when the switch is in the sleeping period and in turned-off condition. Finally, the output voltage can be found as shown below:

$$V_0 = V_i/(1 - D) \tag{5}$$

Here D is the DC-to-DC converter circuit duty cycle. The capacitor C and inductor L selection can be done as:

$$C = D/R(\Delta V_0/V_0)f \tag{6}$$

$$L = D(1 - D)^2 R/2f \tag{7}$$

where R is the consumable load, f is the switch operating frequency and $\Delta V_0/V_0$ is the output voltage ripples.

Fig. 9 represents a four multi-level DC-to-DC boost converter utilized in this work. The primary purpose of using power electronics converters

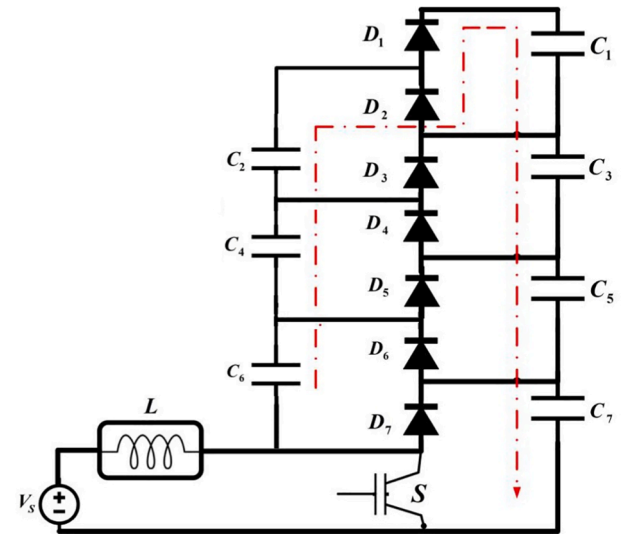

Fig. 11. Four level boost converter - During off mode (switch OFF) the capacitors start charging through the diodes.

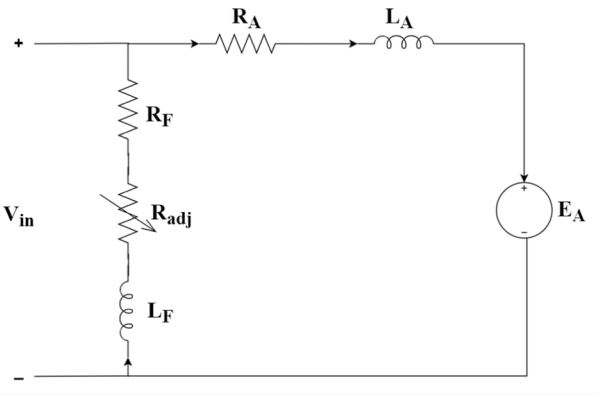

Fig. 12. DC shunt motor equivalent circuit.

is to generate boosted voltages at different levels. Moreover, it is deployed to mitigate and reduce the output ripple which could enhance and improve the overall system stable performance. Besides its other benefits like low harmonic distortion, low voltage tension, low EMI noise, moderate switching frequency with high efficiency, the objective can be achieved by adding capacitors and diodes to the previous configuration (See Fig. 8) to get a four-level output converter for this work:

$$A = 2N - 1 \tag{8}$$

where N represents the number of the output levels, and A is the number of capacitors. Note seven diodes and seven capacitors are needed for this configuration [20].

The aforementioned four multi-level boost converter is analyzed using its two modes of operation. The first one is its ON mode where $T_1 = DT_S$ and the second mode is its OFF mode where $T_2 = (1-D)T_S$. During the ON mode (switch ON), the odd numbered capacitors charge the even ones this implies that C_7, C_5, C_3 charge C_2, C_4, C_6 (See Fig. 10). During off mode (switch off), the capacitors start charging through the diodes (See Fig. 11). Firstly, C_7 will charge through D_7. This causes D_5 to be forward biased and thus C_5 and C_6 will also charge. Then D_3 will conduct to charge C_3 and C_4. Finally, D_1 will conduct to charge C_2 and C_1. This leads to the charging of all capacitors.

In reference to the previous discussion and figures during the ON and OFF modes it can be concluded that the output voltage equals the summation of the capacitors voltages as seen in (9). Moreover, during the ON mode operation, the inductor voltage equals the source voltage (10). During the OFF mode, the inductor voltage equals the difference between the source voltage and the capacitors voltage (11). Furthermore, the voltage is averaged across the inductor (12).

$$V_o = N\mathrm{x}V_C \tag{9}$$

$$V_L = V_S \tag{10}$$

$$V_L = (V_S - V_C) \tag{11}$$

$$V_L|_{ON} + V_L|_{OFF} = 0 \tag{12}$$

By substituting the findings in (10)–(11) into (12) gives:

$$DV_S|_{ON} + (1-D)(V_S - V_C)|_{OFF} = 0 \tag{13}$$

From (13), V_s can be stated as:

$$V_S = V_C(1-D) \tag{14}$$

Substituting (14) in (9) to get voltage equation for N level DC-to-DC converter as:

$$V_o = \frac{\mathrm{N}\,V_S}{1-D} \tag{15}$$

Considering a lossless system:

$$V_S Is = V_o I_O \tag{16}$$

Substituting (15) into (16) gives:

$$V_S Is = \frac{\mathrm{N}\,V_S}{1-D} \tag{17}$$

Simplifying it further gives:

$$Is = \frac{\mathrm{N}}{1-D} I_O \tag{18}$$

DC shunt motor

In DC shunt machine, the field winding is attached in parallel with

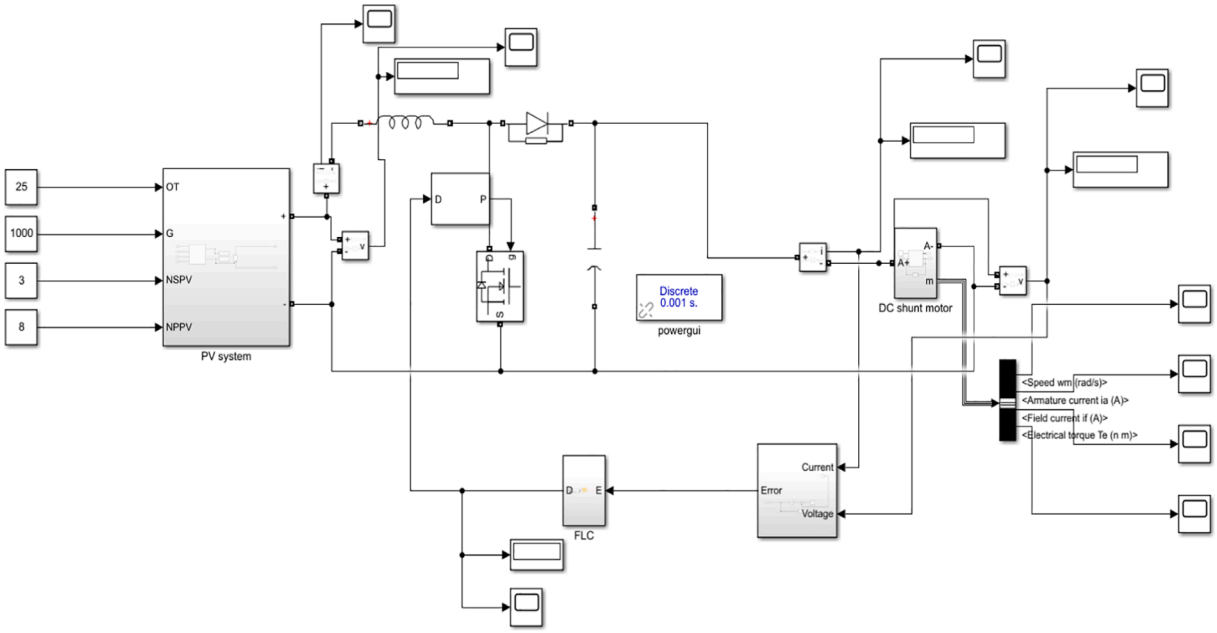

Fig. 13. Implementation of the proposed system in MATLAB SIMULINK.

Table 2
PV module specifications.

No.	Parameter	Value
1.	Cell Number	54
2.	Nominal Power	220.5 W
3.	Open Circuit Voltage	36.3 V
4.	Short Circuit Current	7.84 A
5.	Temperature Coefficient (Isc)	0.0032%/deg.C
6.	Temperature Coefficient (Voc)	–0.123%/deg.C
7.	Number of Parallel Strings	3
8.	Number of Series-Connected Modules/String	8

the rotor winding (armature circuit) as shown in Fig. 12. DC shunt machine translates the electrical DC power into mechanical power manifested in the torque and the speed. This operation is called as the electromechanical energy conversion. Additionally, DC motors translates the electrical energy inductively into mechanical rotational movement without using an intermediate circuit. A DC motor drives the rotation of a shaft by magnetic fields generated by an electrical current flow, which is fed into the rotor by an external feeding DC source through brushes or through an electronic means. The rotation of the shaft is dependent on a brushless DC motor. Electrical input DC voltage changing the field resistance or inserting a resistance with the armature windings circuit can influence the overall performance of the DC shunt motor. These mechanisms are used primarily for controlling the speed of the DC shunt motor and thus influencing the final output torque speed characteristics of the DC shunt motor.

The DC shunt motor nonlinear dynamical mathematical model representation is described below [21].

$$K\phi = \sum_{n=1}^{7} \alpha_n {i_f}^{7-n} = \alpha_1 {i_f}^7 + \alpha_2 {i_f}^6 + \cdots + \alpha_7 \tag{19}$$

$$L_f \frac{di_f}{\mathrm{dt}} = V_f - i_f(R_f + R_{adj}) \tag{20}$$

$$L_a \frac{di_a}{\mathrm{dt}} = V_a - i_a R_a - \mathrm{K}\phi\omega \tag{21}$$

$$\mathrm{J}\frac{\mathrm{d}_\omega}{\mathrm{dt}} = \mathrm{K}\phi i_a - T_l \tag{22}$$

where L_a is the inductance of the armature circuit, i_a is the armature circuit current, V_a is the armature circuit voltage, R_a is the armature circuit resistance of winding, L_f is the field circuit inductance, i_f is the filed circuit current, V_f is the field voltage, $R_f\mathrm{R_f}$ is field circuit resistance of winding,R_{adj} is field circuit adjustable resistance, ω is the angular speed, $\mathrm{K}\phi$ is the DC Shunt motor flux and T_l is the motor torque. Note (19)–(20),V_a equals V_f since the field circuit and the armature circuit are connected in shunt. At the same time in (21)–(22), $K\phi(Wb)$ varies nonlinearly with i_f of the DC shunt motor. Moreover, it is approximated using sixth order polynomial.

Implementation and evaluation

The implementation and evaluation of the proposed scheme is presented in this section. The simulation results of the DC shunt motor connected to the PV panel and controlled by FLC MPPT is presented. The performance is analyzed with variable mechanical torque and different sun insolation levels. The completed circuit implemented in the MATLAB SIMULINK environment including the PV panel, DC-to-DC converter, fuzzy controller, and DC shunt motor is shown in Fig. 13. First, a series of interconnected PV cells (approximately 54) are usually used to construct panels. Panels are connected in a series or parallel to produce the required output voltage and current. This is called as a module. Parameters of PV module are listed in Table 2.

Characteristic curves with insolation levels

PV voltage/current and power/voltage with various insolation levels are shown in Figs. 14 and 15 respectively. Note these figures are aimed to show the maximum capacity or size of the PV system used to supply to the motor. Fig. 14 shows the voltage and current relationship. At 100% insolation level, the current and voltage at MPPT are 24.57A and 239.2 V. At 80% insolation level, the current and voltage at MPPT are 19.65 A and 236.8 V respectively. And at 50%, they are 12.8 A and 226.4 V respectively. Fig. 14 can be referred for all these insolation levels. Fig. 15 shows the power and voltage relationship. At 100% insolation level, it shows the amount of power and voltage at MPPT as 5877.144 W and 240 V respectively. At 80% insolation level, power and voltage at MPPT are 4653.12 W and 236.8 V respectively. At 50% insolation level, power and voltage are recorded as 2780.2 W and 226.4 V respectively. Note Fig. 15 depicts the size of the PV panel at various irradiance levels and does not concentrate on the controller error.

After PV panel parameters were configured with the required parameters, the DC-to-DC buck boost converter was also configured to produce the required output voltage of 240 V, which passed as input to the DC shunt motor. The output ripples for both current and voltage are assumed to be 0.1% and all DC-to-DC buck boost converter parameters are listed in Table 3.

Finally, a DC shunt motor with the specifications listed in Table 4 is chosen, and a step change in mechanical torque is applied to observe the motor's dynamic performance.

Characteristic curves with insolation levels

This section shows the performance of fuzzy controller with insolation levels.

In Fig. 16 and Fig. 17, the torque changed from 20 Nm to 10 Nm at 100% insolation level. It shows here the step change in load torque and operating point. The fuzzy controller shows the ability to handle and control the DC shunt motor transient response during torque changes. The initial DC shunt motor speed is 1743 rpm and the controlled duty cycle is 0.501645. After the load torque has changed from 20Nm to 10Nm, the duty cycle has changed in order to trigger the DC-to-DC

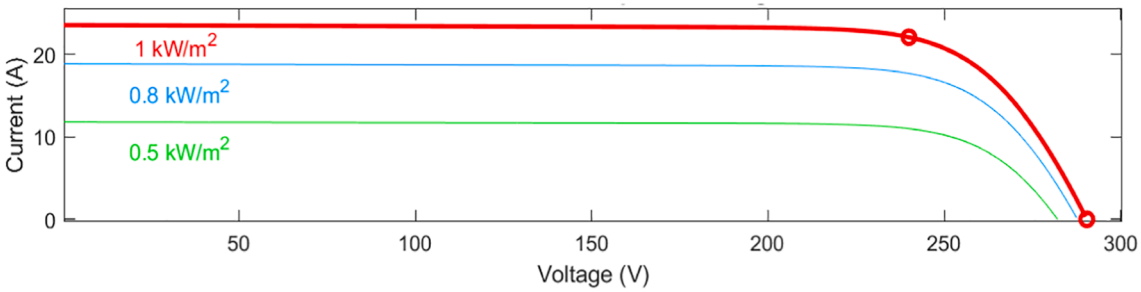

Fig. 14. Current/voltage characteristic curve.

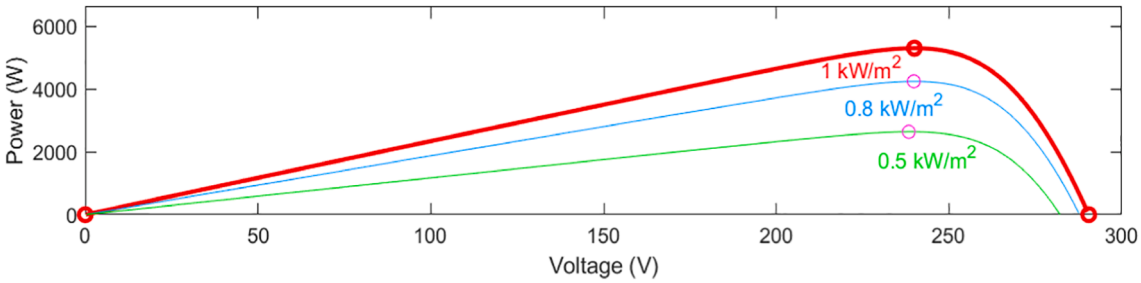

Fig. 15. Power/voltage characteristic curve.

Table 3
DC-to-DC buck boost converter specifications.

No.	Parameter	Value
1.	Input Voltage	240 V
2.	Capacitance	500uF
3.	Inductance	1.26uH
4.	Switching Frequency	10KHz

Table 4
DC shunt motor specifications.

No.	Parameter	Value
1.	Power	5HP
2.	Armature Voltage	240 V
3.	Field Voltage	150 V
4.	Rated Speed	1750RPM

converter. The converter controls the DC shunt motor input to be 238.4 V to achieve the MPP required by the motor. The field current remains constant at 1.07A and the armature current changed from 20.8191 A to 11.0044 A. The PV terminal current is changed from 23.2512A to be 12.2900A after applying torque change.

In Fig. 18 and Fig. 19, the torque changed from 20Nm to 10NM at 80% insolation level. The fuzzy controller shows the ability to handle and control the DC shunt motor transient response during torque changes. The initial DC shunt motor speed is 1720 rpm and the controlled duty cycle is 0.504025. After the load torque has changed from 20Nm to 10Nm, the duty cycle has changed in order to trigger the DC-to-DC converter. The converter controls the DC shunt motor input to be 236 V to achieve the maximum power point required by the motor. The field current remains constant at 1.07A and the armature current changed from 17.0282A to 8.9980A. The PV terminal current is changed from 18.5891A to be 9.8228A after applying torque change.

In Fig. 20 and Fig. 21, the torque changed at 50% insolation level. The fuzzy controller shows the ability to handle and control the DC shunt motor transient response during torque changes. The initial DC shunt motor speed was 1623 rpm, and the controlled duty cycle was 0.513267. After the load torque has changed from 20 Nm to 10 Nm, the duty cycle has changed to trigger the DC-to-DC converter. The converter controls the DC shunt motor input to be 225.6 V to achieve the maximum power point required by the motor. The field current remains constant at 1.07A and the armature current changed from 11.3359A to 5.9824A. The PV terminal current is changed from 11.3359A to be

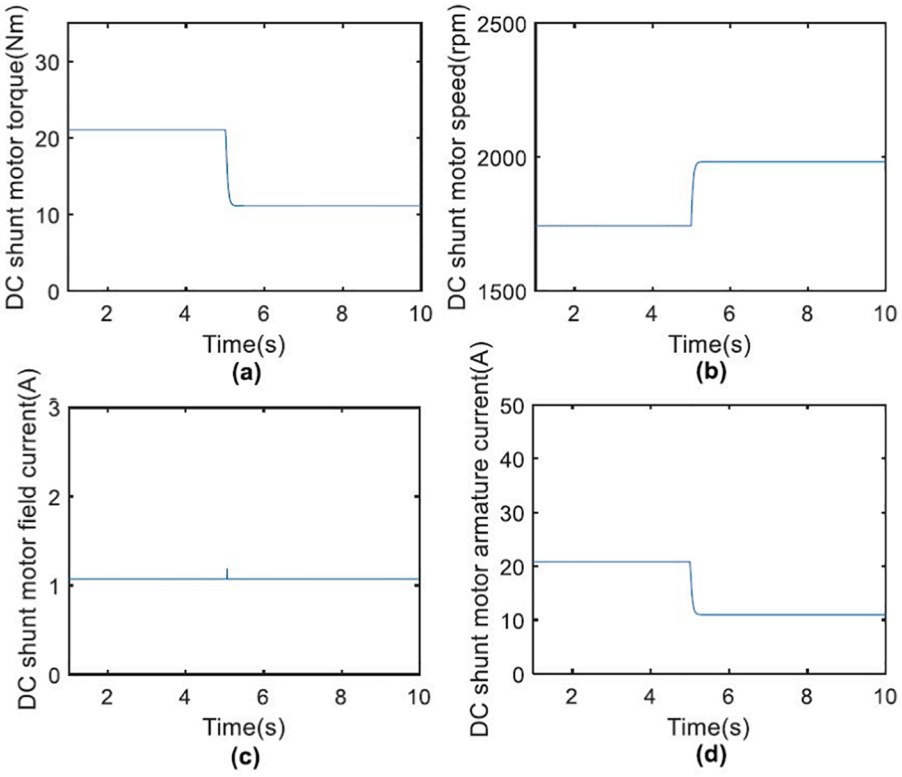

Fig. 16. (a) Torque, (b) speed, (c) motor field current, and (d) armature current while considering the torque step change at 100% of full sun radiation level.

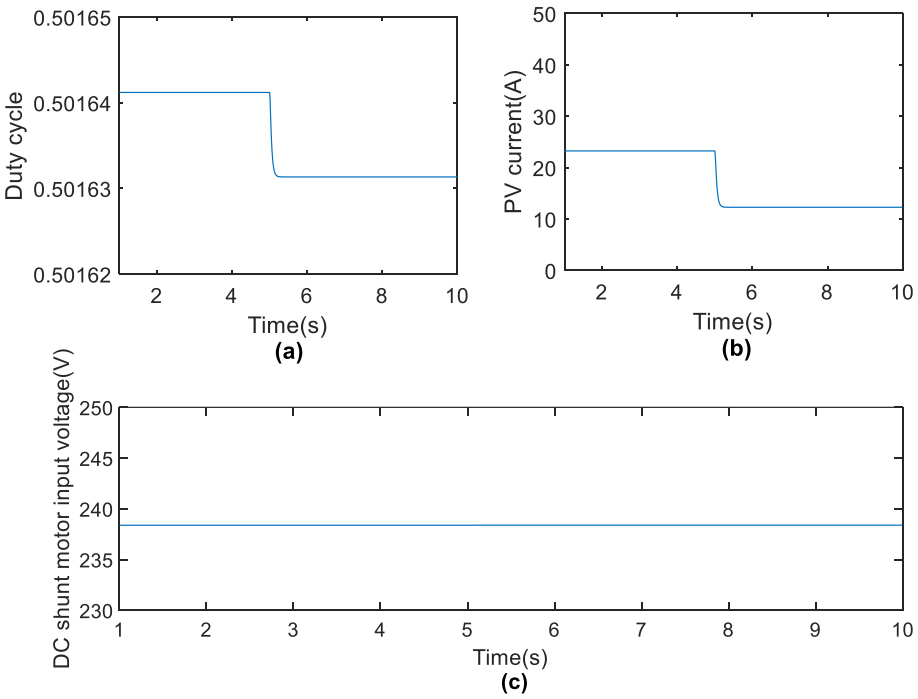

Fig. 17. (a) Duty cycle, (b) PV current, and (c) motor input voltage while considering the torque step change at 100% of full sun radiation level.

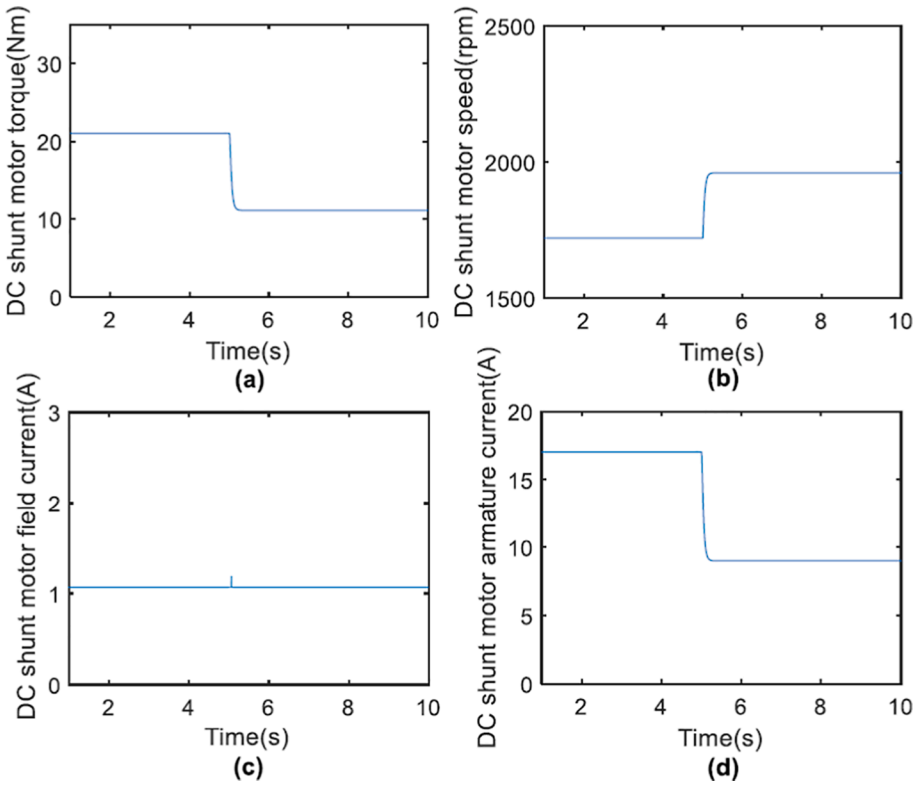

Fig. 18. (a) Torque, (b) speed, (c) motor field current, and (d) armature current while considering the torque step change at 80% of full sun radiation level.

5.9824A after applying torque change.

For all three cases analysed, the voltage 238.4 V, 236 V, and 225.6 V are the PV terminal voltages. These terminal voltage values are bound to change to maintain the torque change. Note that nominal speed 1750 is the rated speed for the 5 horsepower (HP) motor. When the motor load is decreased to 10Nm, the speed is increased to 2000 rpm.

Conclusion

A fuzzy logic controller is used as a MPPT system to perform transient analysis of a DC shunt motor operated by a PV panel. With load torque variation, motor output is evaluated while considering different insolation levels, beginning with 100% of maximum insolation and

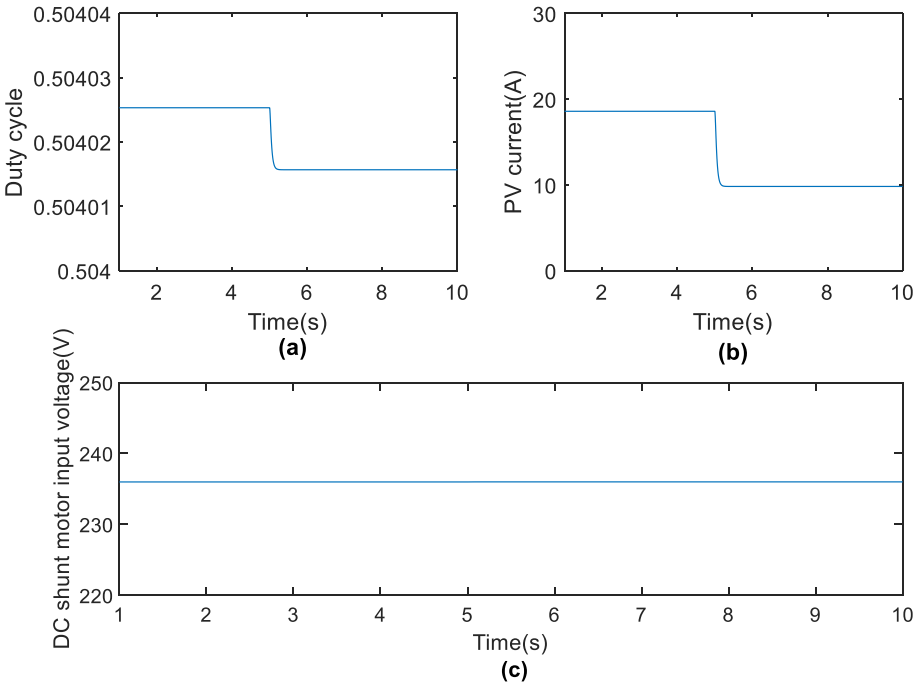

Fig. 19. (a) Duty cycle, (b) PV current, and (c) motor input voltage while considering the torque step change at 80% of full sun radiation level.

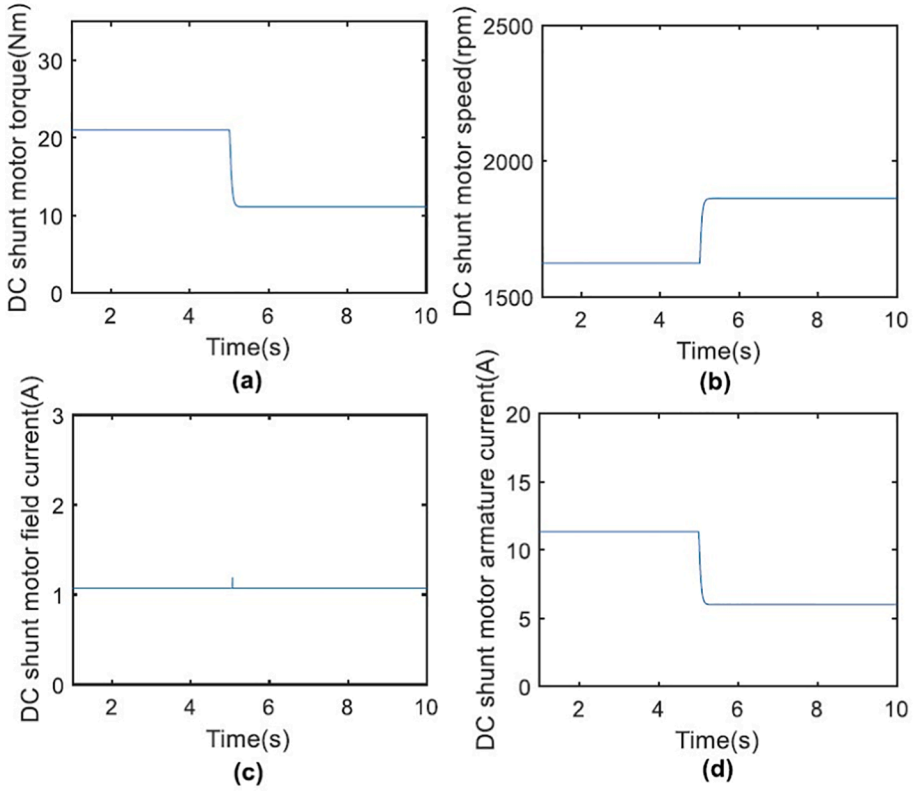

Fig. 20. (a) Torque, (b) speed, (c) motor field current, and (d) armature current while considering the torque step change at 50% of full sun radiation level.

following through 80% and 50%. While studying the dynamic analysis, it has been observed that in all these percentages of maximum insolation, FLC-based MPPT shows the ability to track the necessary power and meet the targeted motor input voltages. Under the step change in motor torque, the duty cycle adjusted to regulate the armature current and maintain the motor input voltage at an appropriate level. The motor field current remained constant as the torque increased but the motor speed got decreased and vice versa. Overall, employing FLC technique as MPPT can withstand the DC shunt motor's performance under varying loads and insolation levels which reflect the system integration robustness and reliability. Future work will be extended towards implementation of ANFIS system and inter-leaved chopper circuit.

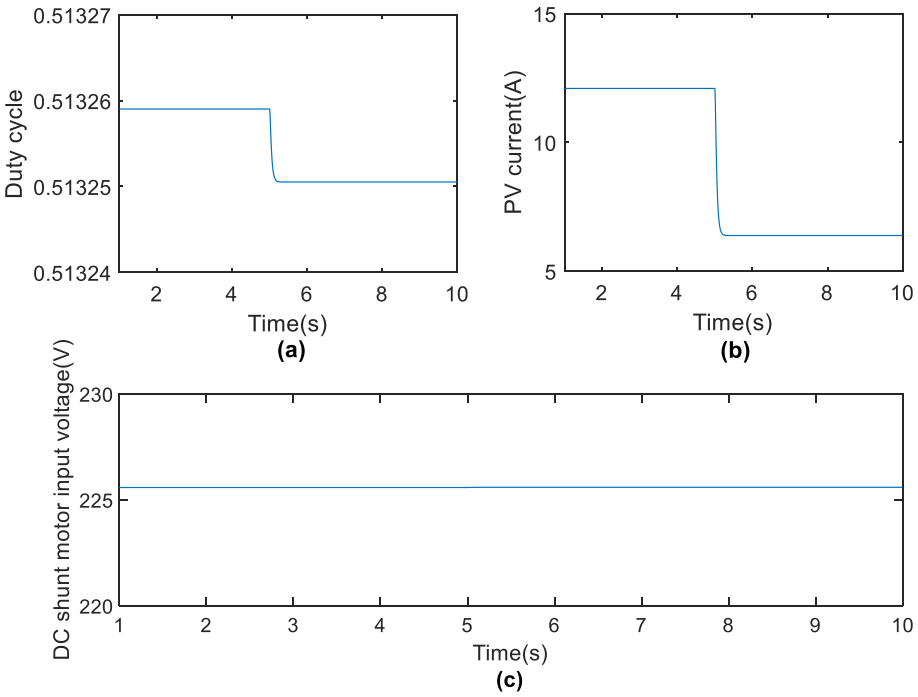

Fig. 21. (a) Duty cycle, (b) PV current, and (c) motor input voltage while considering the torque step change at 50% of full sun radiation level.

Declaration of Competing Interest

The authors declare that they have no known competing financial interests or personal relationships that could have appeared to influence the work reported in this paper.

Acknowledgment

The publication of this article was funded by Qatar National Library.

References

[1] Giatrakos GP, Tsoutsos TD, Mouchtaropoulos PG, Naxakis GD, Stavrakakis G. Sustainable energy planning based on a stand-alone hybrid renewabl eenergy/ hydrogen power system: application in Karpathos island, Greece. Renewable Energy 2009;34(12):2562–70.

[2] Aljdaeh E, Kamwa I, Hammad W, Abuashour MI, Sweidan T, Khalid HM, et al. Performance enhancement of self-cleaning hydrophobic nanocoated photovoltaic panel in dusty environment. *MDPI–Energies* 2021;14(20):6800.

[3] Hammad W, Sweidan TO, Abuashour MI, Khalid HM, Muyeen SM. Thermal management of grid-tied PV system: a novel active and passive cooling design-based approach. IET Renew Power Gener 2021;15:2715–25.

[4] Rekioua D, Matagne E. Optimisation of photovoltaic power systems, medialization, simulation and control, *Springer*, pp 223–273, 2012.

[5] Eltawil MA, Zhao Z. MPPT techniques for photovoltaic applications. Renew Sustain Energy Rev 2013;25:793–813.

[6] Piegari L, Rizzo R. Adaptive perturb and observe algorithm for photovoltaic maximum power point tracking. IET Renew Power Gener 2010;4(4):317.

[7] Sweidan TO, Widyan MS. Perturbation and observation as MPPT algorithm applied on the transient analysis of PV-powered DC series motor, *International Renewable Energy Congress (IREC)*, pp.1–6, 2017.

[8] Widyan MS, Al Tarabsheh AI, Etier IY, Hanitsch RE. Dynamic and steady-state characteristics of DC machines fed by photovoltaic systems. Int J Model Simul 2010;30(3):353–60.

[9] Sweidan TO, Abuashour MI, Osman NF. Transient analysis of DC shunt motor supplied by stand-alone PV system employing FOCV for MPPT, *Advances in Science and Engineering Technology International Conferences (ASET)*, Dubai, United Arab Emirates, pp. 1–6, Februay 2020.

[10] Goetzberger A, Hoffmann V. Photovoltaic solar energy generation. Germany: Springer; March 2005. p. 85–100.

[11] Ross TJ. Fuzzy Logic with Engineering Applications, second ed, *John Wiley & Sons Ltd*, pp. 120–165, 2004.

[12] Chekired F, Larbes C, Rekioua D, Haddad F. Implementation of a MPPT fuzzy controller for photovoltaic systems on FPGA circuit. Energy Procedia 2008;6: 541–9.

[13] Lalouni S, Rekioua D, Rekioua T, Matagne E. Fuzzy logic control of stand-alone photovoltaic system with battery storage. Power Sources 2009;193(2):899–907.

[14] Houssamo I, Locment F, Sechilariu M. Maximum power tracking for photovoltaic power system: development and experimental comparison of two algorithms. Renewable Energy 2010;25(10):2381–7.

[15] Larbes C, Cheikh SMA, Obeidi T, Zerguerras A. Genetic algorithms optimized fuzzy logic control for the maximum power point tracking in photovoltaic system. Renewable Energy 2009;34(10):2093–100.

[16] Khaehintung N, Pramotung K, Tuvirat B, Sirisuk P. RISC-micro-controller built-in fuzzy logic controller of maximum power point tracking for solar-powered light-flasher applications, *30th Annual Conference of IEEE Industrial Electronics Society*, 2004. IECON 2004, Busan, Korea (South), vol. 3, pp. 2673–2678, November 2004.

[17] Louganski KP. Modeling and Analysis of a DC power distribution system In 21st century airlifters, *M.Sc. Thesis*, Electrical Engineering Dept., Faculty of the Virginia Polytechnic Institute and State University, September 1999.

[18] Abu-Qahouq J, Batarseh I. Generalized analysis of soft-switching DC-DC converters," *IEEE 31st Annual Power Electronics Specialists Conference*, Galway, Ireland, pp. 185–192, 2000.

[19] Woywode O, Güldner H. Application of statistical analysis to DC-DC converter. Int Power Electron Conf 2000;121(5):557–62.

[20] Samat MNA, Ponniran A, Kasiran MAN, Yatim MH, Noor MKR, Jumadril JN. Modular multi-level DC-DC boost converter for high voltage gain achievement with reduction of current and voltage stresses. Int J Integr Eng 2021;13(2):32–41.

[21] Ong CM. Dynamic simulation of electric machinery, *Prentice Hall PTR*, Upper Saddle River, New Jersy 07458, pp. 1–220, 1998.